Proceedings of the ASME 2022 International Mechanical Engineering Congress & Exposition
IMECE2022
October 30 – November 3, 2022, Columbus, OH

IMECE2022-95962

Heat Transfer Characteristics of Particle Flow Through Additively Manufactured (SS 316L) Lattice Frame Material Based on Octet-Shape Topology

Youssef Aider
Department of Mechanical Engineering
Mississippi State University
Mississippi State, MS USA

Ashreet Mishra
Department of Mechanical Engineering
Mississippi State University
Mississippi State, MS USA

Like Li
Department of Mechanical Engineering
Mississippi State University
Mississippi State, MS USA

Heejin Cho
Department of Mechanical Engineering
Mississippi State University
Mississippi State, MS USA

Prashant Singh
Department of Mechanical Engineering
Mississippi State University
Mississippi State, MS USA

Abstract

This paper presents experimentally obtained heat transfer characteristics of additively manufactured lattice frame material based on Octet-shaped unit cell. Binder jetting technology was used to print lattices in Stainless Steel 316L material. Lattice porosities ranging from 0.75 to 0.9 were investigated where thermal transport characteristics were obtained for void space occupied by air and particles. Particle diameters were varied from 266-966 microns. Effective thermal conductivity and averaged heat transfer coefficient was calculated through steady-state experiments. It was found that presence of lattice enhances the effective thermal conductivity by 2-4 times when compared to packed bed of particles alone. Furthermore, for gravity-assisted particle flow through lattice panel, significantly high convective heat transfer coefficients ranging from 200-400 W/m^{2}K were obtained for the range of particle diameters tested. The superior thermal transport properties of Octet-shape based lattice frame material for particle flow through them makes it a very promising candidate for particle-to-supercritical carbon dioxide (sCO_2) heat exchanger in concentrating solar power (CSP) application.

1. INTRODUCTION

Supercritical CO_2 (sCO_2)-based Brayton cycle has the potential for higher efficiency (>50%) compared to steam-based Rankine cycles at concentrating solar power (CSP) relevant temperatures [1], due to relatively simpler turbomachinery involved with sCO_2, offering lower installment, maintenance, and operational costs [2]. CSP Gen3 technology identifies three pathways, viz. molten salt, gas-phase and falling particle [2]. Liquified nitrate salts can be operated at temperatures upto 565ºC [3] while chloride salts can go upto 700ºC [2], however, corrosion to stainless steel medium is of major concern in the case of chloride salts [4]. In context with the above drawbacks of molten salt, particles are considered an attractive solution. Particles such as bauxite and silica sand can be heated directly in the receiver section through a heliostat field upto 1000ºC [5]. Heated particles can then be driven with the help of gravity from the central receiver to a particle storage container or directly to a heat exchanger. Particle-to-sCO_2 heat exchangers have been identified as one of the most crucial components demanding innovation to achieve the CSP Levelized Cost of Electricity (LCoE) targets of $0.05/kWh by 2030 [2]. The simplest particle heat exchangers can be in the form of tube bundles, where the fluid such as air or water passes inside the tubes and a heated packed bed of particles is driven around the tubes, thus heating the fluid. This type of heat exchanger is known to have highly localized heat transfer coefficient in which only the sides of the tubes benefit from the movement of the packed bed while the top and bottom of each tube get low heat transfer due to what is known as stagnation and void zones of the packed bed movement [6]. More efficient heat exchangers such as shell-and-plate and shell-and-tube have also been considered for particle-to-fluid applications. Tian et al. [7] suggested a new tube shape to be implemented into the tube-and-shell particle heat exchanger.

Their study showed that the elliptical like tube shape can improve the transfer by up to 53% compared to the conventional circular shape reaching heat transfer coefficient of 250 W/m^{2}K. Experimental study done by Maskalunas et al. [8] showed that the heat transfer coefficient between silica particles and the surface of a parallel plate heat exchanger can reach 350 W/m^{2}K. Parallel plate heat exchangers can be easily manufactured from high performance materials such as stainless steel and zirconium carbide composite for high temperature and pressure applications. These materials can be diffusion bonded to create very compact heat exchangers known as printed circuit heat exchangers (PCHEs) [4].

In this study, a novel enhanced heat transfer concept is developed for the falling particle channel side of the particle-to-sCO_2 heat exchanger for potential employment in a shall-and-plate type heat exchanger. The convective heat transfer coefficient on the falling particle side is enhanced by packing the parallel plates with Octet-shaped lattices. The Octet unit cells and the enclosing plates were additively manufactured in Stainless Steel 316L via. Binder jetting technology. The Octet lattice has been chosen after carrying out direct simulations which quantified its superior heat transfer enhancement characteristics compared to other common unit cell topologies [9].

Following sections present details of different experimental setups employed to measure effective thermal conductivity of lattices made from Octet unit cells where void space is packed with particles of varying diameter, forced convection setup to quantify overall convective heat transfer coefficient of sandwich-type Octet panel with air as working fluid. Finally, a unique test facility was built to carry out particle-based heat transfer experiments. Post this section, the results are presented and analyzed. The paper concludes with major findings from this comprehensive experimental program and path forward based on these findings.

2. EXPERIMENTAL SETUPS AND MEASUREMENT TECHNIQUES

Effective thermal conductivity experiments were carried out on the additively manufactured lattice frames for two different cases: a) void space was occupied by air, b) void space was occupied by particles. Further, convective heat transfer capabilities of single cell thick lattice for air and particle flows have been investigated experimentally. Three different experimental setups were built to measure above-mentioned quantities. Following sub-sections provides details of the experimental setups, tested configurations, and measurement techniques.

2.1 Effective thermal conductivity setup

The effective thermal conductivity (k_{eff}) setup is shown in Fig. 1. A steady-state heat transfer experiment was developed to obtain the k_{eff} of additively manufactured samples. The samples with three different porosities are shown in Fig. 2. A unidirectional heat flow was achieved from top plate to bottom plate of the sample, where Octet-shaped unit cells were sandwiched between the two plates. A cold thermal reservoir was created with the help of an ice-water slurry which was periodically stirred to avoid thermal stratification. An aluminum slab (10 x 10 x 2.5 cm^3) was then partially submerged into the chilled reservoir which acted as a near-constant cold reservoir, owing to its large thermal mass. The lattice sample was made from a 5 x 5 array of Octet-shaped unit cells in the span and the test sample was one unit cell thick. The Octet unit cell was contained in a Cube of edge length 10 mm. Three samples of as design lattice porosities (γ) of 0.75, 0.8 and 0.886 were tested for effective thermal conductivity. The actual porosities of the additively manufactured lattices were 0.733, 0.798, 0.884, respectively. Porosity of lattice structures has a dominant effect on the k_{eff} for a given solid-fluid pair, hence it is imperative that accurate measurements of porosity be carried out in such studies since deviations from as designed and AM-assisted samples are frequent.

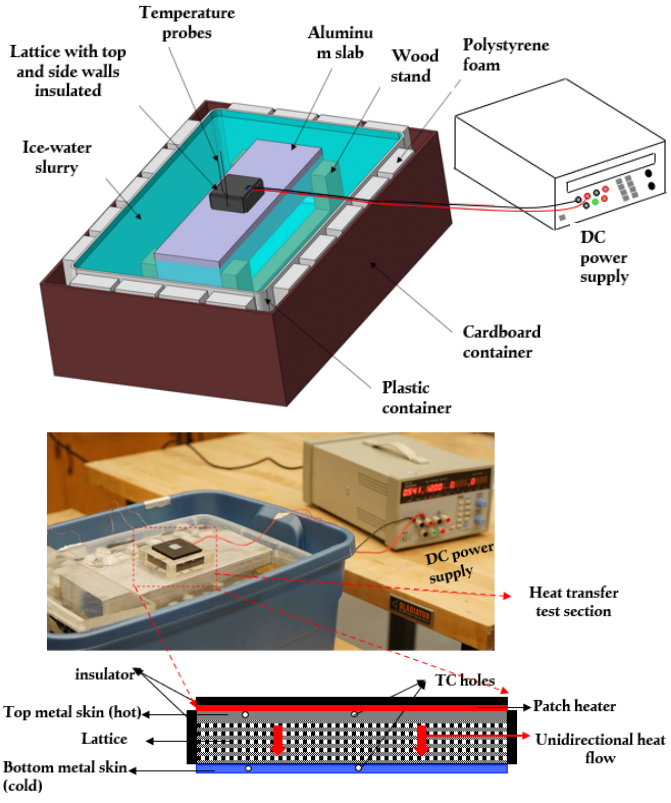

Fig. 1 Experimental setup for k_{eff} determination (top), unidirectional heat flow obtained via patch heater and cold sink (bottom)

It can be seen that the actual porosities differ from the intended ones (Fig. 2), and the deviation is attributed to AM process – a

trend observed in many prior research efforts [10,11]. It is noted that the AM samples have inherent roughness and defects at both the fibers and endwall, however, the measurement of porosity of such structure accounts for all the defects. For k_{eff} experiments in particular, the void space is occupied by stagnant air/particles, hence the AM induced defects is not expected to have an added contribution on k_{eff}, other than the porosity itself. Hence k_{eff} results are reported as a function of measured porosities of the AM parts shown in Fig. 2.

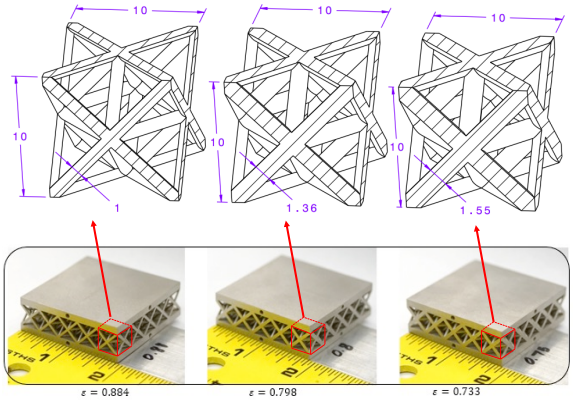

Fig. 2 Three samples of different porosities tested for effective thermal conductivity (also indicated are the designed versus actual porosities), dimensions in top figure in mm.

The effective thermal conductivity (k_{eff}) was determined using Fourier's law of conduction (Eq. 1). A constant heat flux boundary condition was maintained at the top wall of the sample while the bottom wall was glued firmly with the Aluminum slab which served as the cold reservoir. Steady-state heat transfer experiments were conducted at three different heat flux values, and effective thermal conductivity was determined for each case, to ensure that the determined value was independent of the applied heat flux at the top wall. The net heat conducted across the one-unit cell thick sample was calculated by subtracting the stray heat loss from the total heat supplied.

$$k_{eff} = \frac{(q_{cond}/A)\Delta z}{\Delta T} = \frac{(\{q_{total} - \sum q_{loss}\}/A)\Delta z}{\tilde{T}_{top} - \tilde{T}_{bot}} \quad (Eq.1)$$

$$\sum q_{loss} = \frac{k_{ins}}{t_{ins}}\left[A\left(T_{Top,in} - T_{Top,out}\right) + 4b\Delta z\left(T_{side,in} - T_{side,out}\right)\right] \quad (Eq.2)$$

where, "A" is the lattice base area, "Δz" is the thickness of single unit cell of lattice and "b" is the edge length of square cross-sectioned lattice. The stray heat loss venues involved the top wall insulation and the four side wall insulations. Thin thermocouples were secured at the inner and outer skins of the insulation to calculate the stray heat loss, with the knowledge of the thermal conductivity of the insulation material (Eq. 2). This accounting of the heat loss ensured that the reported effective thermal conductivity is only a contribution of the unit cell topology, solid- and fluid-phase thermal conductivities, and lattices' effective porosity.

2.2 Forced convection setup with air as working fluid

Figure 3 shows the schematic of the experimental facility used in the present study where air was the working fluid under forced convection scenario. Air was drawn from a compressed air tank maintained at ~ 1MPa. A pressure regulator was installed downstream of the compressor to adjust the mass flow rate to a desired value. Air was then directed to an orifice plate for flow metering. Differential pressure across the orifice plate static air pressure upstream of the orifice plate and air temperature were measured using Dwyer 477AV-2 (0-10 kPa), Dwyer DPG-002 (0-100 kPa) and fast response T-type thermocouple, respectively. These pressure and temperature measurements were then fed into an in-house MATLAB code to determine the mass flow rate. The metered flow was then passed through a control valve regulating the flow into the test section. The transition of the flow from circular pipe to square duct was executed with the help of a trapezoidal shaped-diffuser.

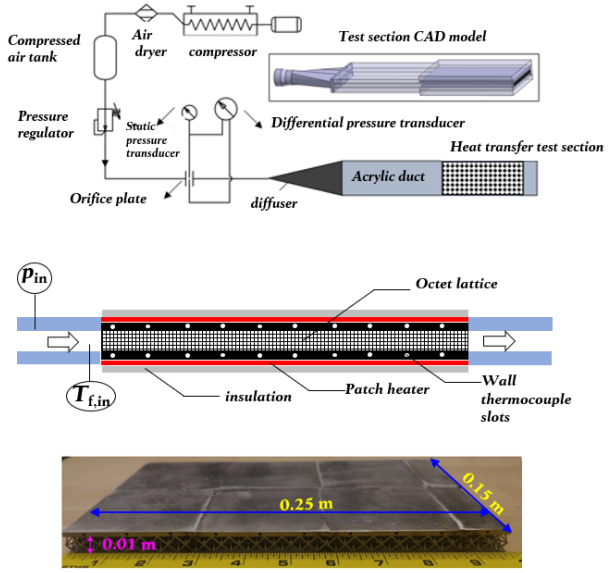

Fig. 3 Assembly drawing of air-based forced convection setup (top), schematic of the instrumentation at the heat transfer test section (middle), additively manufactured sandwich-type Octet panel (bottom)

Figure 3 also shows the schematic of the heat transfer test section. The sandwich panel was heated with patch heaters attached to both the top and bottom walls using thermally conductive silicone compound (CHEMPLEX ® 1381 DE). Rubber foam thermal insulation with thermal conductivity of 0.037 (W/mK) and thickness of 3.2 mm was pasted on the

surface of the heaters. The temperature difference across the insulation was measured at different locations in the panel span to measure the heat losses. T-type thermocouples were used to measure the temperature inside each thermocouple slot which was very close to the solid-fluid interface and this temperature was treated as the representative wall temperature in the convective heat transfer coefficient calculations. A constant heat flux type thermal boundary condition was created with the help of the patch heaters mentioned above, where the heating power was controlled with variable transformers with voltage indicators.

The sandwich panel featuring an array of Octet unit cells had top and bottom walls of 15 cm x 25 cm dimension and thickness was 10 mm (excluding the top and bottom wall thicknesses). Hence, the flow channel had high aspect ratio (width/height) of 15. It is generally challenging to achieve a uniform hydrodynamically developed flow at the entrance of the test section with such a high aspect ratio. To address this, a ~ 33 cm long plexiglass duct was installed between the heat transfer test section and the trapezoidal diffuser. This was done to ensure that the reported heat transfer coefficient in the entry region of the test section does not have a contribution of under-developed nature of the approaching flow.

The samples used in this part were made from reticulating Octet unit cell in span where the sample was one unit cell thick. The sample was additively manufactured from Stainless Steel 316L using binder jetting technology. The bed size of the 3D printer limited the maximum size of the lattice which can be printed in one run. To this end, the sandwich panel show in Fig. 3 was obtained by 3D printing different smaller sections and then joining them together by Tungsten Inert Gas (TIG) welding. A stainless steel 316 filler was used to bridge the gaps between the 3D printed parts, hence creating a seamless thermal bridge between the different sections with excellent thermal contact. The assembled heat exchanger had solid walls with multiple thermocouples holes to allow temperature measurement at different locations inside the walls.

The steady-state heat transfer experimental procedure included heating both top and bottom panels via the glued patch heaters and such that first steady state was achieved, where the air flow through Octet panel was not allowed. Post this step, the air flow rate corresponding to a desired channel flow velocity was set through the heated test section, which was then allowed to cool down since the air supply ~20℃. Once the second steady-state was reached (with continuous airflow), the measurements of flow inlet temperature, wall temperature at discrete locations, and temperature drop across the insulation were carried out. Note that the panel was 15 cm wide and 25 cm long, and a representative wall temperature would only be found by measuring local wall temperatures at several discrete locations on both the top and bottom walls.

An array of 10 equi-spaced thermocouple slots was incorporated (in the AM phase itself) at spanwise locations of W/2 and W/6, at both top and bottom walls, where W is the width of the panel. Under the assumption that the temperature distribution would be symmetric about the channel centerline in the streamwise direction, the representative wall temperature at a particular streamwise location was then obtained by calculating the area-averaged temperature based on the two measurements carried at the span of W/2 (centerline) and W/6. A trendline for streamwise variation of wall temperature was obtained for both top and bottom walls, to get a continuous variation ($T_w(x)$) from the discrete measurements. Convective heat transfer coefficient at these discrete locations along the streamwise direction is given as,

$$h(x) = \frac{q"_{conv}}{T_w(x) - T_f(x)} \quad (Eq. 3)$$

where, $q"_{conv} = (q_{total} - q_{loss,insulation})/A$, and local fluid temperature, $T_f(x) = T_{f,in} + \left(q"_{conv} W/\dot{m}c_p\right)x$. Here, q is heat transfer, A is heated areea, W is channel width, $\dot{m}$ is air mass flow rate, c_p is specific heat capacity of air. The local convective heat transfer coefficient ($h(x)$) obtained from above procedure was then used to calculate a representative $\tilde{h}$ for each row of unit cells in the streamwise direction.

2.3 Particle heat transfer test facility

The heat transfer test section described in Section 2.2 (Fig. 3, bottom) above was used in the experiments for determination of convective heat transfer coefficient with particles as working fluid. Unlike air-based convection experiments, the particles which carry heat from the test section had to be transported back into the system. To this end, a bucket elevator-system was designed, developed, and built for these experiments. Buckets elevator works by rotating a set of buckets attached to a chain or a belt, and by doing so, the buckets scoop the particles from the bottom of the elevator casing and discharge them at the top.

The acutal assembled test facility, assembly CAD model, instrumented heat transfer test section, and schematic representation of heat transfer scenario involving falling particles are shown in Fig. 4. Particles are first stored at room temperature in the top hopper while the top and bottom walls of the sandwich panel was being electrically heated with set of patch heaters. The particles were held until the panel walls reached a temperature of ~100ºC. A gate valve was installed right downstream of the heat transfer section, which facilitated the on/off type flow of particle across the heat transfer test section. Once the desired panel wall temperatures were achieved, the gate valve was flipped and the elevator was started at the same time, to allow the transport of the spent particle back into the top hopper via a series of equi-spaced buckets.

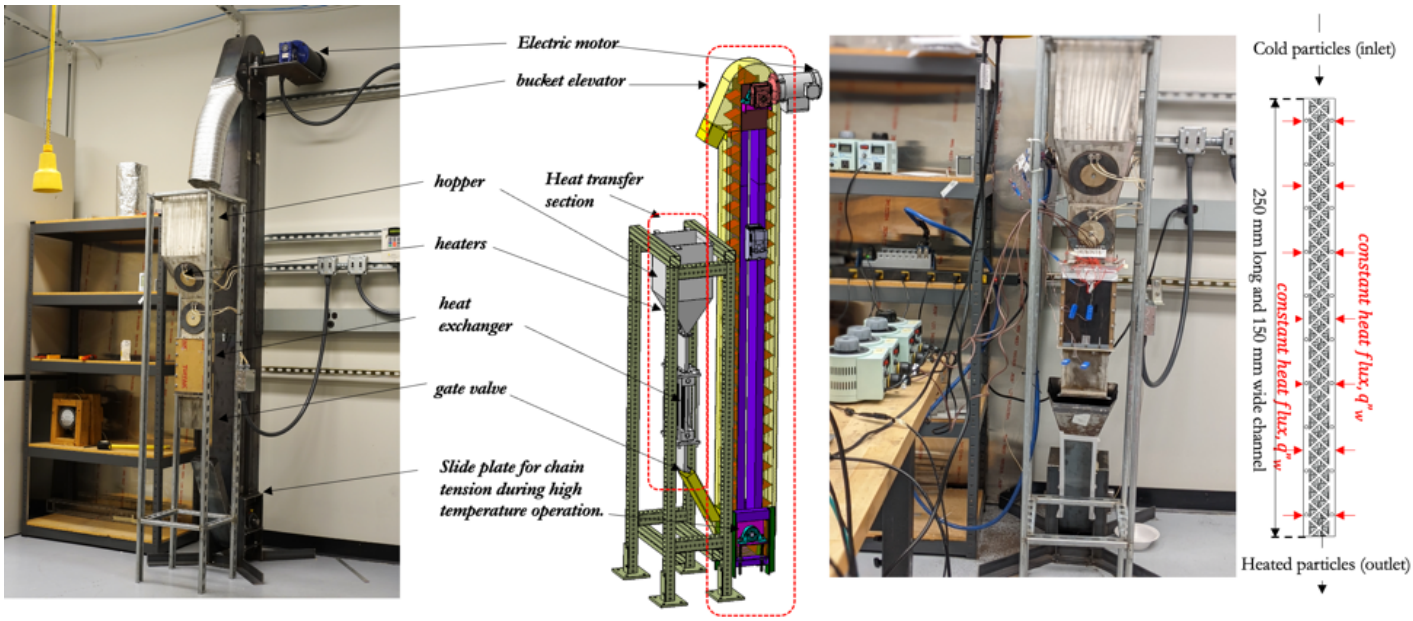

Fig. 4 Particle heat transfer test facility

It should be noted that particle heat transfer experiments are different from the air-based experiments in the sense that the working fluid was recirculated and fed back into the heat transfer section. Due to convection, particles carry away some heat from the heated walls and the same batch of particles is transported back into the hopper above the test section via the bucket elevator. During the transport in the buckets, the particles loose some heat to the laboratory ambient, however, in our initial testing and the design of heat transfer experiments, we observed that the particle temperatures continue to keep increasing as they are recirculated for a prolonged duration. Further, it was decided that bucket-elevator-based experiments should not be allowed to run for very long periods of time, as particles can get destroyed/crushed during the transport, which may inherently change the particle size distribution with time, and a satisfactory steady state could never be achieved, both in the sense of heat transfer and the working fluid rhealogical properties.

To address the above aspect, a novel quasi-steady state heat transfer methodology was devised exclusively for this part of the investigation, which could effectively provide local convective heat transfer coefficient where heat transfer was facilitated through falling particles. In this approach, firstly the hopper is filled with desired type of particles where the total mass of particles was decided such that a packed bed flow could be achieved at the heat transfer test section. Once the hopper was charged with particles, the heating process was started where all the eight patch heaters occupying the entire 150 x 250 mm^2 panel on both left and right sides of sandwiched panel were heated. Once the steady-state heat transfer condition was achieved, the particle flow rate through the Octet panel was initiated by opening the gate valve installed at the bottom of the heat exchanger to 100%. Note that this facility also allows a fine control over the particle flow rate through the gate valve while still maintaining a packed moving bed through the Octet panel. In this study, the maximum possible particle mass flow rate was studied, hence 100% opening of the gate valve was set. Prior to the particle flow start, the data acquisition system was initiated which involved over 20 thermocouple measurements across the heat transfer test section, including a pair of temperature measurements for particle inlet and outlet. Once the particles started to flow through the Octet panel, the walls of the panel started to cool down rapidly to a local minima. At that point onwards, the particle and the wall temperatures continued to slowly increase for the remainder of the transient experiment. The reason behind this phenomena is explained above. In the heat transfer coefficient calculation, the wall and particle temperatures during this slow heat ramp up period was taken into consideration and the local instantaneous convective heat transfer coefficient was determined through the following eqation:

$$h(x,t) = \frac{q"_{conv}(t)}{T_w(x,t) - T_f(x,t)} \quad (Eq.4)$$

where, $q"_{conv}(t)$ is the heat convected away from the walls via the particles in motion and this was obtained by subtracting the local heat losses from the backside of the eight patch heaters occupying and supplying constant heat flux on the left and right sides of the panel. Note that the temperature drop across the insulation material was measured at multiple locations along the streamwise length and also recorded along with the wall temperature at the same fequency throughout the transient operation. The heat loss however was minimal compared to the total heat supplied.

2.3.1 *Particle type and size distribution*

The particles used in the experiment are made from sintered bauxite. Three different particle batches were tested: CARBOBEAD-CP 40/100 with a mean particle diameter of 266 µm, CARBOBEAD-CP 30/60 with a mean particle diameter of 397 µm, and CARBOBEAD HSP 20/40 with a mean particle diameter of 966 µm. Particle size analysis was performed using Anton Paar PSA 1190 LD particle size analyzer.

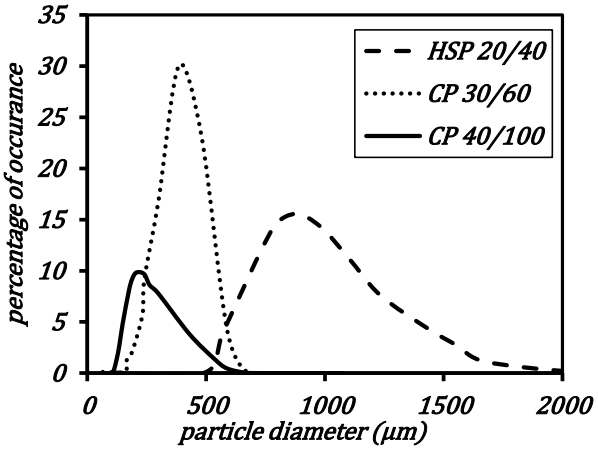

Fig. 5 Particle size distribution

The particle size distribution is shown in Fig. 5. For other thermo-physical and spectral properties of these particles, the readers are reffered to [12-14].

3. RESULTS AND DISCUSSION

In this section, we are presenting experimental results on effective thermal conductivity, convective heat transfer coefficient for air and particles as working fluids.

3.1 Effective Thermal Conductivity (k_{eff})

Effective thermal conductivity experiments were carried out for three cases, a) packed bed of particles, b) lattice with void space occupied by air, c) lattice with void space occupied with particles. Each configuration was tested at three different heat flux levels to ensure that the reported k_{eff} values were independent of the heating conditions. Note that the wall temperatures at these three different heat flux levels was ranging between 20-50℃, hence radiation effects and other solid-phase thermo-physical property changes can be ignored. Figure 6 shows the k_{eff} for packed bed of particles. It was observed that the packed bed k_{eff} was similar for all particles with diameters varying between 266-966 μm with an averaged value of ~ 0.4 W/mK.

The 2nd set of experiments were conducted on Octet lattice with void space occupied by air. Figure 7 shows the k_{eff} values for the three lattice samples with actual porosities varying from 0.733 to 0.884. The thermal conductivity of solid-phase was measured to be ~13 W/mK. The effective thermal conductivity averaged over three different heat fluxes, $\tilde{k}_{eff}$ was found to be a strong function of porosity, and found to vary as 1.49, 1.203, and 0.795 W/mK for lattice actual porosities of 0.733, 0.798, and 0.884, respectively. In this case as well, the k_{eff} was independent of the applied heat flux.

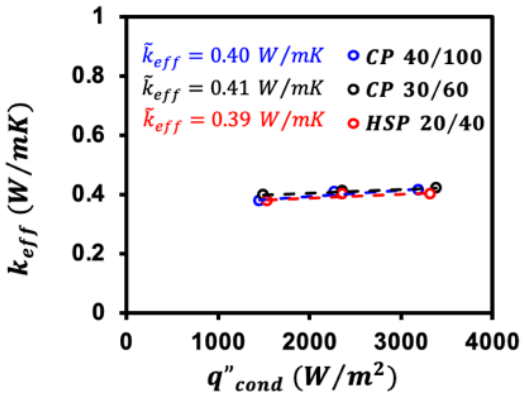

Fig. 6 Effective thermal conductivity of packed bed of particles

The 3rd set of k_{eff} experiments were conducted on lattices with void space being occupied by the particles with diameters varying from 266 – 966 μm (Fig. 8). There was a clear decreasing trend in the k_{eff} value with increasing lattice porosity, which is again consistent for the case when void space was occupied by air, indicating that particles don't alter the dominant impact of fibers and their intrinsic thermal conductivity values, even though particles are nearly 16 times more thermally conductive than air.

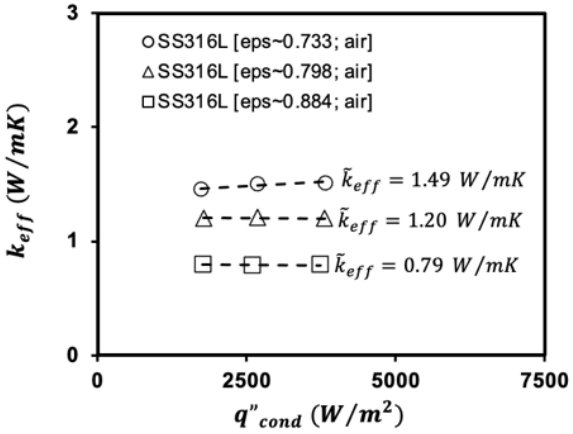

Fig. 7 Effective thermal conductivity of Octet lattice (void space occupied by air)

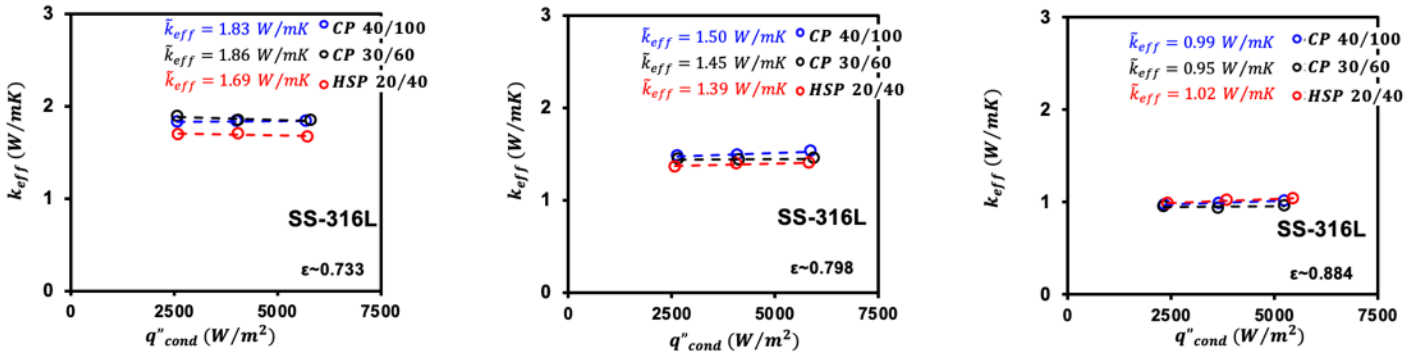

Fig. 8 Effective thermal conductivity of Octet lattice (void space occupied by particles)

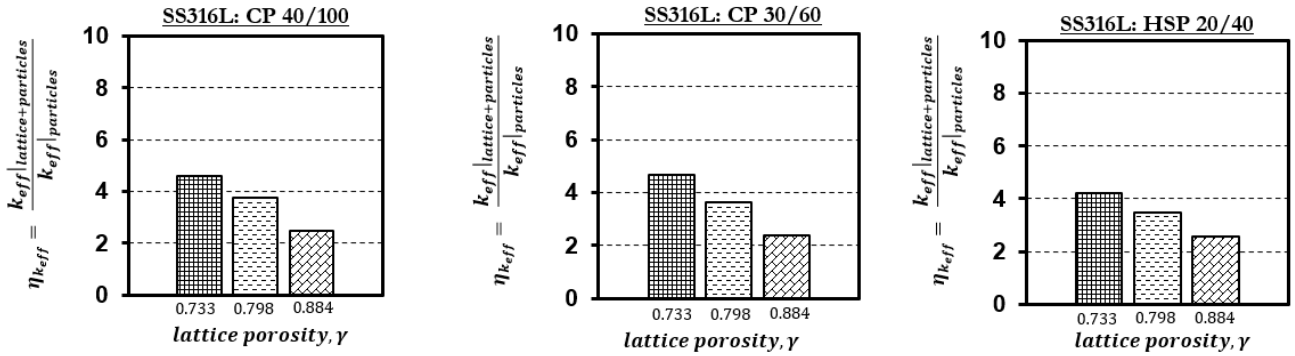

Fig. 9 Effective thermal conductivity enhancement ($\eta_{k_{eff}}$) of Octet lattice packed with particles in reference to packed bed of particles

Figure 9 presents the relative enhancement in k_{eff} values for the lattice when particles were packed in void space in reference to a packed bed of particles. This enhancement in k_{eff} is one mode which implicitly affects the overall thermal transport between the hot and cold sides. Further, a rapid decline in $\eta_{k_{eff}}$ was observed with increasing lattice porosity. The enhancement levels were similar for different particle sizes for the three lattice porosities and varied from 2-4 times compared to the particle packed bed configurations (absence of lattice).

3.2 Forced convection with air as working fluid

This sub-section presents steady-state experimental results on local convective heat transfer coefficient offered by Octet unit cells when packed between two parallel plates (integrally manufactured) with air as the convective agent (Fig. 10). Air flow condition is presented in terms of Reynolds number ($Re = \rho u d_h/\mu$), where ρ is the density, u is the flow velocity, d_h is the channel hydraulic diameter, and μ is the dynamic viscosity. The panel is shown in Fig. 3 and was formed by joining smaller pieces together as the maximum printable size was limited by the manufacturing method.

The Octet lattices offer significant enhancement in heat transfer, both in the developing and developed region, with sustained enhanced heat transfer levels. Hence, the employment of Octet unit cells between two parallel plates is hypothesized to provide significant enhancement in overall heat transfer coefficient of the heat exchanger. A periodic heat transfer behavior was achieved at nearly half of the streamwise distance from the inlet and a gradual increase in heat transfer was observed as the flow exits the channel. This increase is attributed to the exit effects, where the exit plane was directly exposed to laboratory ambient conditions, which assisted in additional cool down of the top and bottom plates. This phenomena led to increased heat transfer coefficient values closer to the exit. For the design of heat exchangers based on the data presented in Fig. 10, users should take the periodic heat transfer region values of h as they are free from both the inlet and exit effects.

It should be noted that in the case of plane channel, the heat transfer coefficient variation with streamwise location would have showed a steep decline and a constant value convergence in very short distance from the inlet.

3.3 Forced convection with particle as working fluid

A developing heat transfer profile was observed with air as working fluid. The hypothesis behind introducing fibrous media between parallel plates carrying particles was that the increase in wetted surface area along with particle-to-fiber and

particle-to-endwall interaction would result in an overall higher heat transfer.

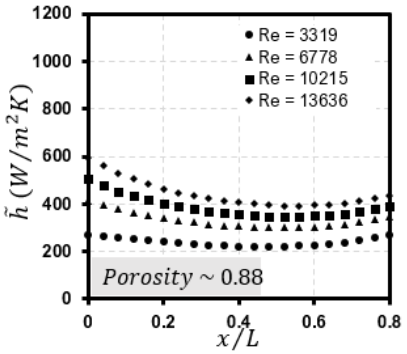

Fig. 10 Local convective heat transfer coefficient variation with lattice porosity

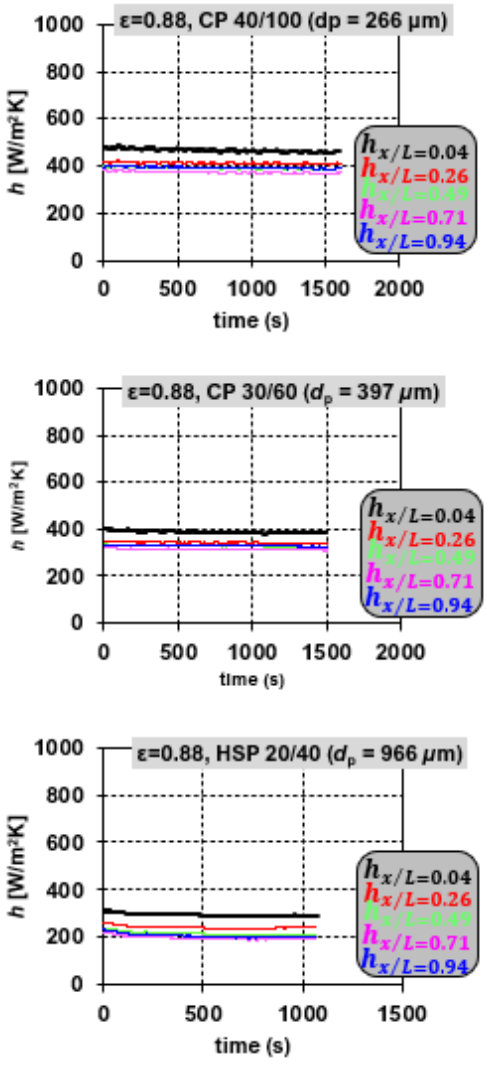

Fig. 11 Transient convective heat transfer coefficient at five different locations in the streamwise direction for three particle types (Octet panel porosity of 0.88)

Our preliminary flow visualization experiments carried out on particles flowing through Octet lattice revealed that the particle flow behviour around the fiber and endwall was similar to that of airflow. Above observation suggested that increased level of heat transfer could be obtained for particle flow through lattice as it was also observed for air flow through lattice. To this end, a novel quasi-steady state heat transfer technique was used to determine time-dependent local convective heat tansfer coefficient by carrying out measurements for over 30 minutes during the slow heat ramp-up phase of the experiment as described in Section 2.3.

Figure 11 shows the transient heat transfer coefficient determined at five discrete locations in the streamwise direction for three types of particle flows through Octet panel of porosity 0.88. Only the highest porosity of panel was chosen since we wanted to study the particle diameter effect on the local heat transfer behavior of Octet panels and that the two lower porosities of the Octet panel (0.75 and 0.8) did not exhibit unobstructred free flow of particles of all the diameters.

The quasi-steady state experiments were carried out for particle diameters ranging from 266-966 microns. It can be observed through the continuous data collection of temperatures that the resultant heat transfer coefficient remained constant in the "quasi-steady" state period. In Fig. 11 the heat transfer data is only shown for the quasi-steady state period, and it should be noted that the wall and particle temperatures continued to rise during this period. Due to closed-loop nature of the test facility, the continued heat addition into the system resulted in slow rise in system's temperature. However, the increase in the local wall and local fluid tempeature was nearly the same at a given time instance, leading to a constant heat transfer coefficient.

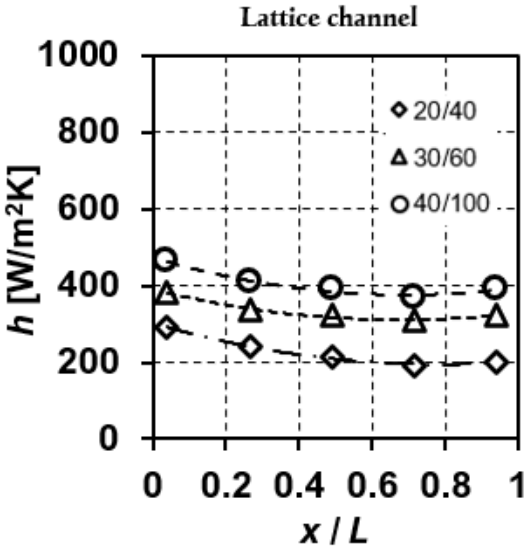

Fig. 12 Time-averaged convective heat transfer coefficient variation with streamwise location (Octet panel porosity of 0.88)

Figure 12 shows the time-averaged convective heat transfer coefficient for particle flows through Octet lattice of 0.88 porosity. Figure 11 demonstrates that such a time-averaging is justified as the heat transfer coefficient was found to be time-independent in the quasi-steady state duration. A developing heat transfer trend was observed for all three types of particles where the inlet region had the highest heat transfer and near-periodic heat transfer behavior was observed at nearly 50% of the streamwise length of the channel. A slight increase was observed towards the exit of the panel and is attributed to cooler air presence right downstream of the panel's exit.

The smallest diameter particle had highest heat transfer coefficient followed by the two other larger particle sizes. Note that these experiments were carried out for the unobstructed particle flow through the Octet panel, i.e. the gate valve at the panel exit was 100% open while particles were still in a moving packed bed scenario. The smallest particle size would consequently result in higher mass flow rates compared to the two higher particle flow rates.

CONCLUSIONS

A comprehensive experimental program has been undertaken here and presented in this paper, to evaluate the heat transfer performance of Octet-shaped unit cells for their capabiltiies to provide convective heat transfer enhancement with air and particles as the working fluids. Octet panels were manufactured via. Binder jetting method using Stainless Steel 316L material. The effective thermal conductivity and averaged heat transfer coefficient was obtained experimentally for the cases where the void space is occupied by air and particles. The following major conclusions have been drawn from this work:

(a) Packing the void space of Octet lattice with particles results in thermal conductivity enhancements ranging from 2 to 4 times that of the packed bed of particles. Maximum benefits were observed for the lowest lattice porosity.
(b) For airflow Reynolds number ranging from 3000-13000, the convective heat transfer coefficients in the period heat transfer region varied between 200-400 W/m^2K.
(c) For particle flow through Octet lattice of porosity 0.88, the convective heat transfer coefficient was ~400 W/m^2K for CP 40/100. A near-constant heat transfer was observed after 40% of the streamwise length.

ACKNOWLEDGMENTS

This material is based upon work supported by the U.S. Department of Energy's Office of Energy Efficiency and Renewable Energy (EERE) under the Solar Energy Technologies Office Award Number DE-EE0009377. This report was prepared as an account of work sponsored by an agency of the United States Government. Neither the United States Government nor any agency thereof, nor any of their employees, makes any warranty, express or implied, or assumes any legal liability or responsibility for the accuracy, completeness, or usefulness of any information, apparatus, product, or process disclosed, or represents that its use would not infringe privately owned rights. Reference herein to any specific commercial product, process, or service by trade name, trademark, manufacturer, or otherwise does not necessarily constitute or imply its endorsement, recommendation, or favoring by the United States Government or any agency thereof. The views and opinions of authors expressed herein do not necessarily state or reflect those of the United States Government or any agency thereof.

REFERENCES

[1] C.S. Turchi, Z. Ma, T.W. Neises, M.J. Wagner, Thermodynamic Study of Advanced Supercritical Carbon Dioxide Power Cycles for Concentrating Solar Power Systems, Journal of Solar Energy Engineering. 135 (2013).

[2] M. Mehos, C. Turchi, J. Vidal, M. Wagner, Z. Ma, C. Ho, W. Kolb, C. Andraka, A. Kruizenga, Concentrating Solar Power Gen3 Demonstration Roadmap, National Renewable Energy Lab. (NREL), Golden, CO (United States), 2017.

[3] Wilson, Graham, et al. "Packed Bed Thermal Storage for LWRs." Storage and Hybridization of Nuclear Energy. Academic Press, 2019. 229-248.

[4] Zhu, Q., Tan, X., Barari, B., Caccia, M., Strayer, A.R., Pishahang, M., Sandhage, K.H. and Henry, A., 2021. Design of a 2 MW ZrC/W-based molten-salt-to-sCO2 PCHE for concentrated solar power. *Applied Energy*, *300*, p.117313.

[5] Ho, Clifford K. "A review of high-temperature particle receivers for concentrating solar power." Applied Thermal Engineering 109 (2016): 958-969.

[6] Hertel, Julian D., and Stefan Zunft. "Experimental validation of a continuum model for local heat transfer in shell-and-tube moving-bed heat exchangers." *Applied Thermal Engineering* (2022): 118092.

[7] Tian, X., Guo, Z., Jia, H., Yang, J. and Wang, Q., 2021. Numerical investigation of a new type tube for shell-and-tube moving packed bed heat exchanger. *Powder Technology*, *394*, pp.584-596.

[8] Maskalunas, Jeffrey, Gregory Nellis, and Mark Anderson. "The heat transfer coefficient associated with a moving packed bed of silica particles flowing through parallel plates." Solar Energy 234 (2022): 294-303.

[9] Kaur, I. and Singh, P., 2020. Flow and thermal transport through unit cell topologies of cubic and octahedron

families. *International Journal of Heat and Mass Transfer*, *158*, p.119784.

[10] Aider, Y., Kaur, I., Cho, H. and Singh, P., 2022. Periodic heat transfer characteristics of additively manufactured lattices. *International Journal of Heat and Mass Transfer*, *189*, p.122692.

[11] Kaur, I., Aider, Y., Nithyanandam, K. and Singh, P., 2022. Thermal-Hydraulic Performance of Additively Manufactured Lattices for Gas Turbine Blade Trailing Edge Cooling. *Applied Thermal Engineering*, p.118461.

[12] Chung, K.M., Zeng, J., Adapa, S.R., Feng, T., Bagepalli, M.V., Loutzenhiser, P.G., Albrecht, K.J., Ho, C.K. and Chen, R., 2021. Measurement and analysis of thermal conductivity of ceramic particle beds for solar thermal energy storage. *Solar Energy Materials and Solar Cells*, *230*, p.111271.

[13] Chen, C., Yang, C., Ranjan, D., Loutzenhiser, P.G. and Zhang, Z.M., 2020. Spectral radiative properties of ceramic particles for concentrated solar thermal energy storage applications. *International Journal of Thermophysics*, *41*(11), pp.1-25.

[14] Siegel, N.P., Gross, M.D. and Coury, R., 2015. The development of direct absorption and storage media for falling particle solar central receivers. *Journal of Solar Energy Engineering*, *137*(4).